Design and Functional Validation of a Mechanism for Dual-Spinning CubeSats

Eric Peters[*], Pratik Dave, Ryan Kingsbury, Anne Marinan, Evan Wise, Chris Pong, Meghan Prinkey,
Kerri Cahoy, David W. Miller, Devon Sklair, Joshua Emig

William J. Blackwell[**], G. Allen, C. Galbraith, R. Leslie, I. Osaretin, M. Shields, E. Thompson,
D. Toher, D. Townzen and A. Vogel

Abstract

The mission of the Micro-sized Microwave Atmospheric Satellite (MicroMAS) is to collect useful atmospheric images using a miniature passive microwave radiometer payload hosted on a low-cost CubeSat platform. In order to collect this data, the microwave radiometer payload must rotate to scan the ground-track perpendicular to the satellite's direction of travel. A custom motor assembly was developed to facilitate the rotation of the payload while allowing the spacecraft bus to remained fixed in the local-vertical, local-horizontal (LVLH) frame for increased pointing accuracy. This paper describes the mechanism used to enable this dual-spinning operation for CubeSats, and the lessons learned during the design, fabrication, integration, and testing phases of the mechanism's development lifecycle.

Introduction

The Micro-sized Microwave Atmospheric Satellite (MicroMAS) project is a three-unit (3U) CubeSat under joint development by the MIT Space Systems Laboratory and MIT Lincoln Laboratory, currently scheduled to launch in May 2014. Its mission to deliver useful images of hurricanes, cyclones, and tropical storms using a low-cost satellite stretches the limit of what has been previously accomplished using the CubeSat platform. The payload is a multispectral passive microwave radiometer that has been developed by MIT Lincoln Laboratory in collaboration with the University of Massachusetts-Amherst. The payload is contained within a standard 1U CubeSat structure, occupying one-third of the total vehicle volume. All spacecraft support functions are integrated within the remaining 2U volume as part of a separate bus structure that has been developed by the MIT Space Systems Laboratory (SSL).

In order to effectively collect data with the radiometer sensor, the spacecraft must simultaneously sweep the radiometer field of view perpendicular to the ground-track while maintaining sub-degree pointing accuracy fixed in the local-vertical, local-horizontal (LVLH) frame. A satellite stabilized in this way is considered a "dual-spinning" spacecraft. Figure 1 illustrates how MicroMAS will be oriented during on-orbit operations. The following sections discuss the development of the mechanism, dubbed the Scanner Assembly (SA), used to enable this motion – including design requirements; early prototypes and design trades; and functional validation.

Motivation for Dual-Spinning Design

Preliminary design analyses[1,2] determined that precessing the angular momentum of an entire spinning CubeSat as it progresses through its orbit would require torque in excess of the capabilities of available commercial, off-the-shelf (COTS) CubeSat mechanisms for attitude control. This includes the MAI-400 unit, developed by Maryland Aerospace, Inc. (Crofton, MD), which was selected for MicroMAS attitude determination and control. The MAI-400 incorporates an attitude computer, a 3-axis reaction wheel set, a 3-axis magnetorquer set, and earth-horizon sensors in a single package.[3] To maintain the spacecraft's alignment with the LVLH frame, MicroMAS would need to slew at a rate equal to the angular velocity of

---

[*] Space Systems Laboratory, Massachusetts Institute of Technology, Cambridge, MA
[**] Lincoln Laboratory, Massachusetts Institute of Technology, Lexington, MA

the spacecraft's orbit. For a simple spinner, the system's angular momentum is simply its moment of inertia about the axis of rotation times its spin rate. Assuming a spin rate of 0.8 Hz and a 500-km orbit, the torque required to slew in this manner exceeds the capabilities of our magnetic torque rods by roughly two orders of magnitude.[1]
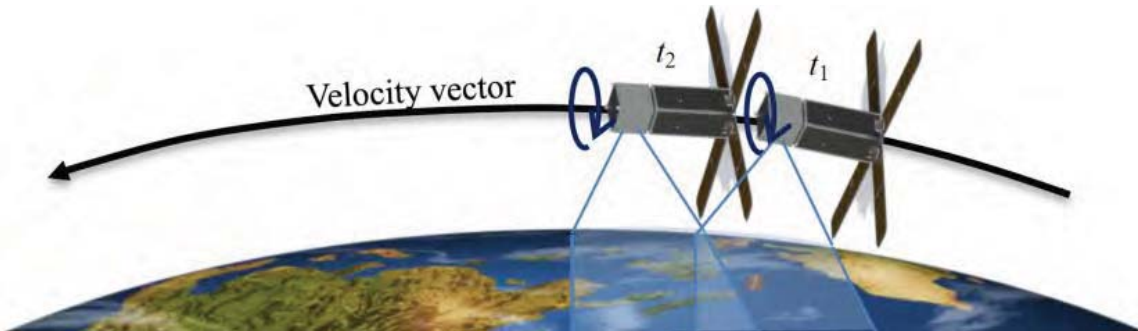

Figure 1. MicroMAS Orbit and Swath Overlap[2]

Since MicroMAS does not possess enough torque to precess the entire angular momentum bias of a simple spinner, it must leave its angular momentum oriented in a constant direction, which is illustrated in Figure 2. Because of this arrangement, a simple spinner version of MicroMAS must exchange the momentum of the spacecraft between internal storage devices (such as reaction wheels) to maintain proper orientation of the radiometer payload as the spacecraft traverses its orbit. At point (c), the momentum storage device would have to account for twice the angular momentum produced by the rotating system. For a simple spinner rotating at 0.8 Hz, this angular momentum would be an order of magnitude greater than the momentum storage capability provided to MicroMAS by the reaction wheels in the MAI-400.[3] Additionally, at points (b) and (d) in the orbit, the momentum storage devices must trade between themselves the entirety of the spacecraft's momentum four times during the course of a single rotation of the spacecraft, which would require a torque nearly five orders of magnitude greater than the maximum torque available to the MAI-400's reaction wheels.[3] No miniature reaction wheel set could realistically transfer momentum fast enough between its wheels to keep a simple spinner aligned with the LVLH frame.[1]
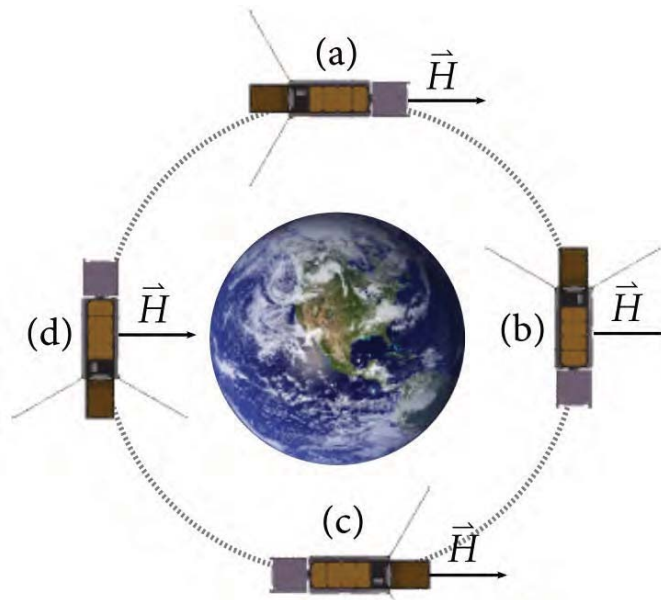

Figure 2. MicroMAS Maintaining LVLH Alignment with Constant Momentum[1]

For these reasons, MicroMAS was designed as a zero-momentum, dual-spinning spacecraft, in which a purpose-designed "scanner assembly" mechanism would provide the actuating mechanical and electrical interface between the spinning payload module and the spacecraft bus fixed in the LVLH frame. Figure 3 provides a system overview of MicroMAS in its dual-spinning configuration.
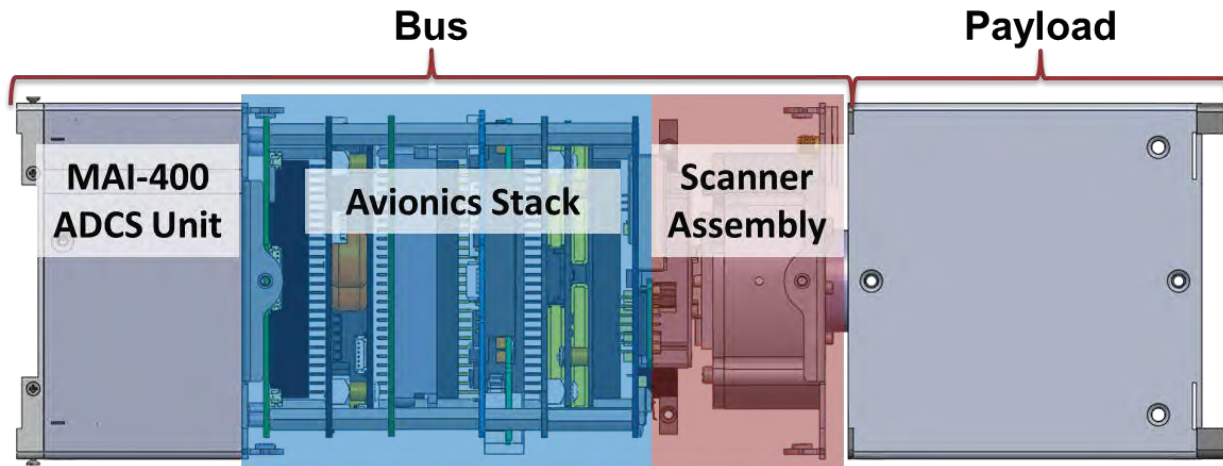

Figure 3. MicroMAS System Overview

It was determined early in the design phase that to ensure mission success, the scanning mechanism would need to possess a specific set of capabilities (presented in Table 1). This list of capabilities was then formalized into specific design requirements, against which the performance of the finalized mechanism could be validated.

Table 1. Scanner Assembly Design Requirements

Requirement	Justification/Rationale
Must fit within a 10 cm by 10 cm by 3.5 cm volume	This ensures that the mechanism fits within the CubeSat cross-section and that all components will fit within the length available in a 2U bus structure
Must be able to continuously operate in a space environment for a nominal mission lifetime of one year.	This is the only system onboard that requires continuous mechanical (rather than electrical) operation
The scanning assembly shall exert a maximum torque less than or equal to 7 mN-m	Maximum torque available at the reaction wheels at 0 rpm is 7.4 mN-m
Must be capable of rotating a 1U, 1-kg payload at a nominal rate of 1 Hz (60 rpm)	Requirement for data collection at target altitude
Must have angular position knowledge to a precision higher than 0.1 deg (6 arcmin)	Minimize error for geolocation accuracy
Must have at least 8 electrical feed-lines	Minimum number of lines required for power/data transfer between bus and payload

Scanner Assembly Design

The design of the MicroMAS scanner assembly (shown in Figure 4) incorporates both COTS and custom-designed hardware in order to satisfy the aforementioned design requirements. Commercial parts include a brushless DC motor (rotor/stator only); an incremental rotary encoder; a thin-section radial ball bearing; and a miniature slip ring capsule. Custom parts were then designed to incorporate the COTS components into a single assembly and provide the necessary mechanical interfaces between the bus and payload structures. The entire assembly fits within the 10 cm x 10 cm x 3.5 cm (3.937 in x 3.937 in x 1.378 in) volume constraints imposed by the design requirements.
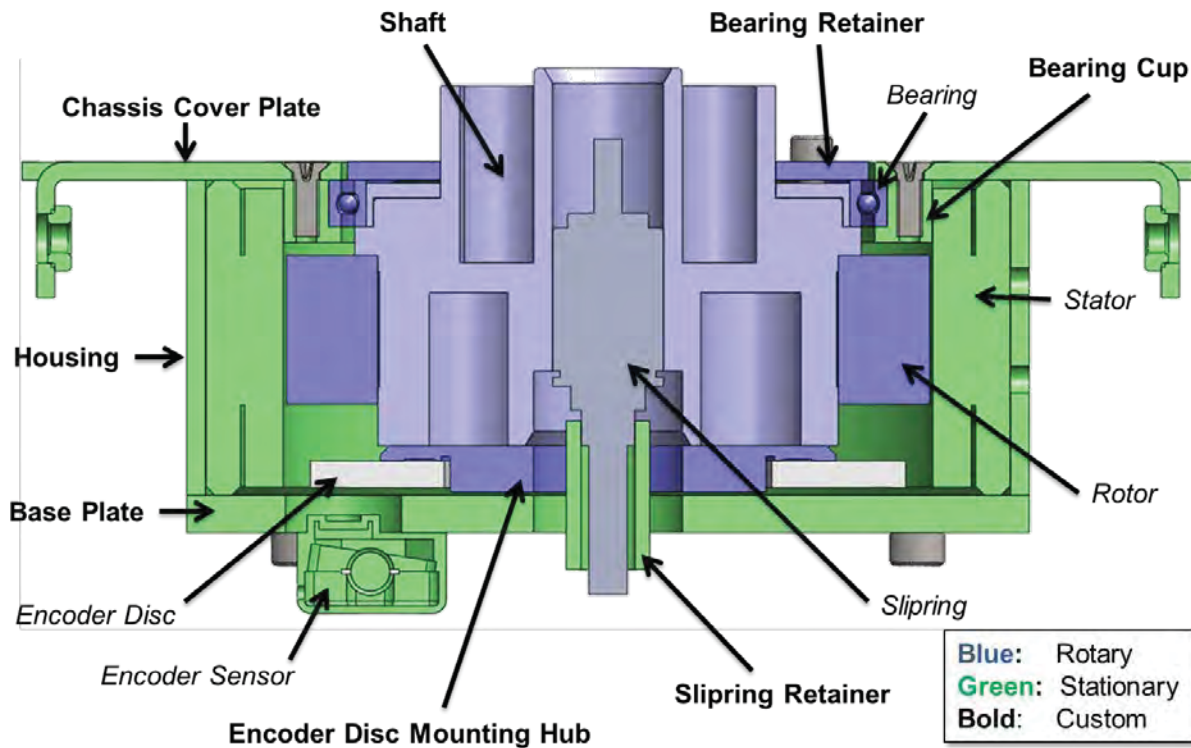

Figure 4. Cross-section view of Scanner Assembly

COTS Component Selection
The need for low-speed vacuum operation led to the selection of a zero-cogging brushless DC motor as the basis of operation for the scanner assembly. A brushless motor was selected over conventional brushed motors because of the electrical arcing that can occur between the brushes during vacuum operation. Furthermore, the low iron content of the zero-cogging rotor allows for smooth rotation at the relatively low speed of 60 rpm. The selected component was an Aeroflex[*] Z-0250-050-3-104 rotor and stator combination, due to its continuous torque capabilities, and large internal bore. Its continuous torque capability of 254 mN-m (36 in-oz) was well above the 7 mN-m operating requirement, leaving the system with a large performance margin for future applications. The dimensions, while not the most compact of all the options surveyed, fit within the design space, though the 2.7-cm (1.060-in) height of the stator necessitated that several components be mounted internal to the assembly.

To provide angular position knowledge, the MicroE[**] M1500V optical rotary encoder system was chosen, for its vacuum operation capability and its available array of optical gratings of various diameters and resolutions.[5] The selected grating has an outer diameter of 5.04 cm (2.0 in), which allows it to be placed

inside of the stator, minimizing the impact on the overall assembly height. Additionally, the chosen grating has a resolution of 7,200 counts per revolution, which on its own leads to an angular position knowledge of 0.05 deg (3 arcmin). Coupled with the 4x interpolation of the encoder head, the system has a total of 28,800 counts per revolution, providing angular position knowledge down to 0.0125 deg (0.75 arcmin).

The Aeroflex[*] CAY-1398 miniature slip ring capsule was selected to provide the electrical interfaces between the bus and payload.[6] With a diameter of 0.95 cm (0.375 in) and an overall length of around 2.5 cm (1 in), the compact size of this unit allowed it to be mounted within the shaft of this motor assembly. Additionally, its twelve electrical lines exceeded the minimum of eight set by the design requirements.

The final COTS component is the bearing. Given the assembly volume constraint and the height already occupied by the stator, cover plate and encoder head, it was determined that only a single bearing could be accommodated in the assembly. This led to the selection of an NHBB[*] deep groove, thin-section radial ball bearing,[7] as it did not need to be mounted in a duplex configuration like angular contact bearings.

Simulations of the spacecraft attitude control system were used to determine the maximum static imbalance of the rotating payload that the system could tolerate before control authority no longer met mission-required levels. From this, the team was able to determine that the CG of the payload had to be within 1.3 mm (0.051 in) of the axis of rotation.[1] The selected bearing is manufactured to Class 5 tolerances as specified by the Annular Bearing Engineering Committee (ABEC 5), which allows for a maximum radial runout of 0.005 mm (0.0002 in), well below the static imbalance requirement.[8] To prevent a loss of contact between the inner race of the bearing and the shaft that would be caused by differential thermal expansion between the steel and aluminum, a stainless steel ring was added to the shaft to serve as the bearing mounting surface. Its diameter was sized to provide a light interference fit of 0.0025 mm (0.0001 in), as recommended by the manufacturer. Furthermore, the height of the mounting ring was sized 0.13 mm (0.005 in) shorter than the bearing height, allowing the inner race of the bearing to be compressed by tightening the ring used to axially retain the bearing on the shaft. The deformations to the inner race caused by the interference fit and the compression serve to preload the bearing and mitigate some of the inherent radial play.

Design Units

The development cycle of the scanner assembly leveraged the use of an iterative design process, using stages of prototypes and engineering models such that any lessons learned and design changes in the current iteration could be integrated into the following iteration. Each prototype served as a risk reduction measure, proving different aspects of the design (and therefore increasing TRL) with each iteration.

3-D Print Unit
Once the basic design of the scanner assembly was established, a 3D printer was used to fabricate mockups of each component (shown in Figure 5). This was done early in the design process in order to identify any issues that may have been overlooked during the initial design. The component mockups were used to visualize the physical envelope of each part in the assembly, check the fit between components (especially those that were custom designed to interface with and between COTS components), visualize the volume of the overall assembly, and most importantly, verify that the unit could be assembled.

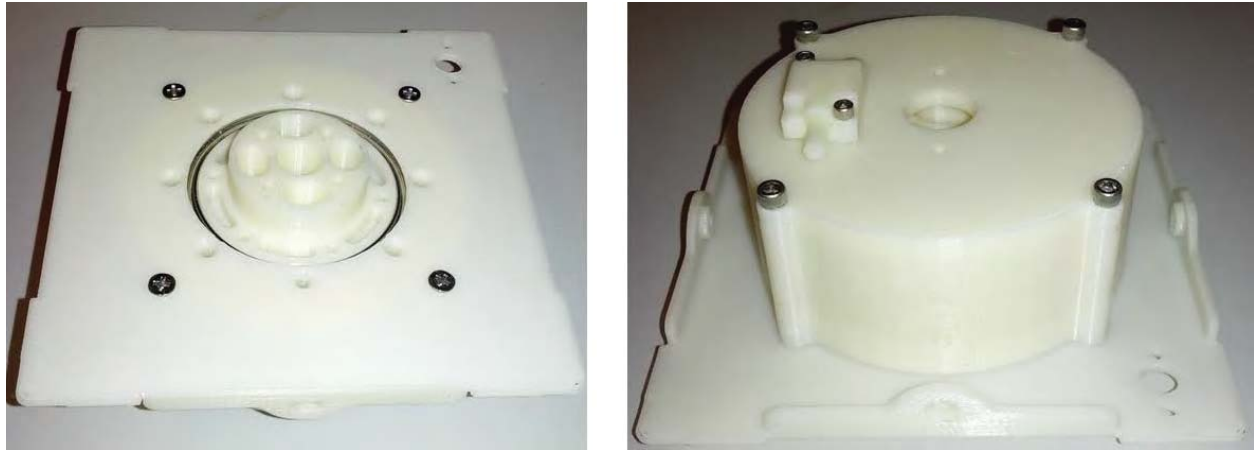[*] New Hampshire Ball Bearings, Inc., Chatsworth, CA

Figure 5. 3-D Printed Scanner Assembly Mockup

Engineering Design Unit

The next unit fabricated was an Engineering Design Unit (EDU). The purpose of this assembly was to verify mass properties of the custom components, assess whether any part posed manufacturing issues, and provide an initial functional unit for early testing and driver development. Due to component lead time, mass mockups for the rotor and stator were used, and functionality was provided through the use of a surrogate motor mounted externally to the assembly, as shown in Figure 6. At this point in the design process, a mass mockup of the satellite – with the Engineering Design Unit scanner assembly joining bus and payload mockups – was subjected to random vibration testing at "qualification" level, as prescribed by GSFC-STD-7000.[9] Post-test inspection of the hardware showed that the glass grating disk did not shatter or separate in any way from the hub to which it was mounted, quelling two concerns that the team had about using a glass grating. Additionally, the shaft still spun freely after the test, showing that the bearing could survive the combined loading imposed by random vibrations and from stowage in a CubeSat deployment device.[*]
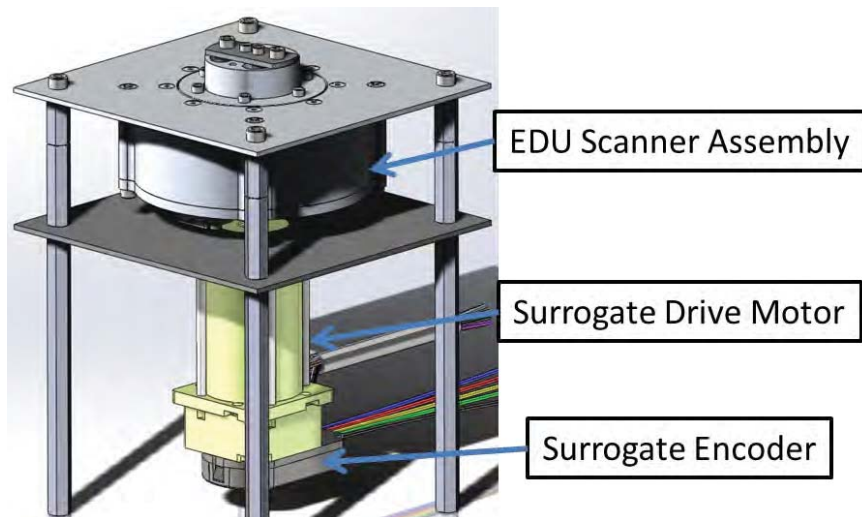

Figure 6. Engineering Design Unit with surrogate drive motor

---

[*] MicroMAS will be deployed by a NanoRacks CubeSat Deployer (NRCSD), which can be seen at <http://nanoracks.com/nanoracks-completes-flight-integration-cubesats-bound-orb1-iss/>.

<u>Engineering Test Unit</u>
After incorporating these design changes, an Engineering Test Unit (ETU) was built utilizing flight-spare COTS components (shown in Figure 7). This unit was used for full functional testing and validation, and also served as a baseline estimate for cost and schedule of the flight-model scanner assembly.

Figure 7. Engineering Test Unit scanner assembly

Structural Validation

Considering the lack of flight heritage of a dual-spinning CubeSat, and the criticality of the scanner assembly to the MicroMAS mission, a broad series of tests were conducted to qualify the mechanism for successful performance in relevant environments. Structural tests and analyses were conducted to identify the most effective method for securing the rotor to the motor shaft, due to concern for loss of contact during thermal expansion/contraction. Three mating methods were evaluated – epoxy, tolerance rings, and mechanical press-fit. Though tolerance rings seemed most directly applicable for the task, a lack of knowledge regarding their space heritage (and a lack of experience using them) resulted in the choice for epoxy securing the rotor and shaft in the flight-model assembly.

<u>Rotor/Shaft Interface Test Units</u>
Occurring in parallel with fabrication of the engineering test unit scanner assembly, a series of tests were conducted to determine which method would be used to secure the rotor to the shaft in the flight unit. This trade was motivated by the concern that differential thermal expansion between the stainless steel rotor and the aluminum shaft would cause a loss of contact between the two parts at the low temperatures.

Calculations were performed to determine the change in rotor and shaft diameters at the expected (cold) operational temperature, along with three temperatures below that operational point. The three classifications of interference fits are presented in Table 2.

Table 2. Diameter ranges for interference fits[10]

Fit Classification	Symbol	Minimum Size Above Basic Shaft Diameter (mm) [in]	Maximum Size Above Basic Shaft Diameter (mm) [in]
Locational Interference Fit	H7/p6	0.026 [0.0010]	0.042 [0.0016]
Medium Drive Fit	H7/s6	0.043 [0.0017]	0.059 [0.0023]
Force Fit	H7/u6	0.060 [0.0024]	0.076 [0.0030]

For the calculations that follow, a worst-case scenario was assumed where the rotor inner diameter was the largest value allowed by the H7 fit class. Table 3 summarizes the material interference between the shaft and the rotor diameters for various temperatures.

Table 3. Change in interference fit between shaft/rotor under various temperature differentials

Temperature (°C)	ΔT (°C)	Interference (mm) [in]	Fit Classification
25	0	0.051 [0.0020]	Medium Drive
0	-25	0.038 [0.0015]	Locational Interference
-10	-35	0.033 [0.0013]	Locational Interference
-15	-40	0.030 [0.0012]	Locational Interference
-25	-50	0.025 [0.00099]	Locational Transition

The results of the above calculations showed that although the press fit mating method would be acceptable for the expected operating temperature range, it did not leave much margin for survival if the system got colder than expected. This led to a study of different mating methods and a series of tests to characterize the performance of the options under consideration.

The two additional mating methods considered were epoxy and tolerance rings. The selected epoxy was Lord 3135, due to extensive institutional knowledge of the product and known flight heritage on the Chandra X-ray Observatory and the Suzaku satellite.[11] A tolerance ring, shown in Figure 8, is a corrugated metal strip specifically designed for mating concentric, cylindrical parts. Sample units were provided by USA Tolerance Rings.[*]

Figure 8. Tolerance ring[12]

The tolerance ring is installed between the shaft and the bore, providing a radial spring force that maintains alignment of the two parts. The rings are available in a wide variety of stock styles and sizes, making them ideal for nearly any combination of loading and geometry. However, the lack of internal experience with this product, coupled with no known flight heritage added two critical risks to this option. Table 4 summarizes the advantages and disadvantages of three methods that were considered.

The press fit method was used in the engineering test unit, and was thus tested through the functional tests the ETU scanner assembly was subjected to. The other two options, epoxy and the tolerance ring, were tested separately. The purpose of this series of tests was to assess the strength of the rotor-shaft interface provided by both methods. This was accomplished by creating two sets of surrogate shafts and rings, with dimensions identical to the flight components. The shaft was made from 6061-T6 aluminum alloy – the same material that the flight shaft would be made from – with a 9.9-mm wide by 0.127-mm deep (0.390 in by 0.005 in) circumferential groove cut into it, as depicted in Figure 9. The initial dimensions for the groove were established by combining required dimensions of both the tolerance ring and the epoxy – the tolerance ring size set the groove width while the recommended epoxy bond line

---

[*] USA Tolerance Rings, Inc., Pennington, NJ

thickness set the groove depth. When testing began, it was found that a deeper groove was needed to fit the tolerance ring. The surrogate ring was made from A513 mild steel with a height of 12.7 mm (0.500 in) and a wall thickness of 1.59 mm (0.0625 in). This material differs from the material of the flight rotor, Custom 455 stainless steel, but its low cost, accessibility, and ease of machining made it the best option.

Table 4. Rotor-mounting Options

|	Press-Fit	Epoxy	Tolerance Ring
Advantages	• No additional parts required • Simple to design	• Flight heritage (ACIS instrument, bond held with ΔT of -145 °C)	• Robust to thermal expansion/contraction • Known torque and radial load capacities
Disadvantages	• Loss of fit with thermal variation • Requires additional equipment for installation	• High CTE • Estimated elastic modulus • Requires careful application, curing	• No prior experience • No (known) flight heritage • Tests needed to get groove fit right
Testing Performed	Thermal testing	Torque testing	Torque testing
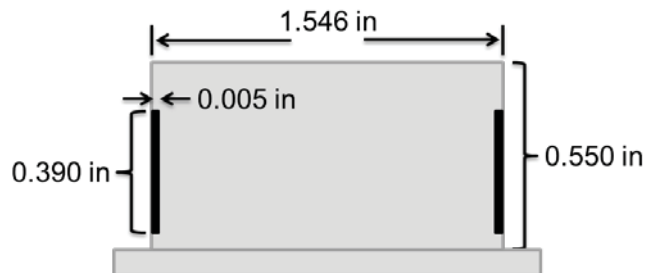
Figure 9. Dimensions of shaft/rotor test rig
(0.390 in = 10 mm), (0.005 in = 1 mm), (1.546 in = 39.2 mm), (0.550 in = 14 mm)

During assembly of the test shafts, it quickly became apparent that the chosen groove depth was too shallow to securely hold the tolerance ring. On the first assembly attempt, the tolerance ring was forced out of the groove when even minimal force was applied to the surrogate rotor ring. Attempts to mate the two pieces with excessive force only served to buckle the tolerance ring. A new surrogate shaft was machined for the tolerance ring unit, this time with a groove depth of 0.056 cm (0.022 in); this depth was selected to fully retain the 0.051-cm (0.020-in) base thickness of the tolerance ring along with 25% of the corrugated portion. The circumference of the ring was trimmed to maintain a gap of 0.15 cm (0.060 in) between edges, which fell within range of 0.10 to 0.20 cm (0.040 to 0.080 in) recommended by the product engineers.

A 1/2-13 bolt was secured through a bore through the center of the test shaft. Flat washers were placed on either side of the bolt and the installation was torqued to 13.6 N-m (120 in-lb). The assembly was then placed in a vise and the jaws were tightened around the ring. A torque wrench was then placed on the bolt head and torque was applied to the assembly. The test procedure continued as follows: (1) Test both units to the peak torque provided by the motor during nominal operations (4 in-lb or 0.5 N-m); (2) If successful, continue application of torque until failure occurs; (3) Note the torque at which the assembly failed.

Both test units survived an applied torque of 7.34 N-m (64.9 in-lb). At this point, the aluminum test shafts suffered material failures where the lock washers dug into the aluminum. After this occurred, the tests were halted and the application of higher torques was not attempted. It is important to note that the neither the epoxy nor the tolerance ring were tested to the point of failure. Post-test analysis showed that the applied torque was an order of magnitude less than the rated torque capacity of 76.3 N-m (675 in-lb) for a ring of that size. For the epoxy shaft, a simple analysis (shown in Equations 1 and 2) converted the applied torque to shear stress at the interface between the shaft and the epoxy layer. Results showed that the applied torque caused a shear stress of 303 kPa (44 psi) in the epoxy layer, which is nearly two orders of magnitude lower than the epoxy's rated shear strength of 26 MPa (3800 psi).

$$F = \frac{\tau}{r} = 374 \text{ N (84 lbf)} \tag{1}$$

$$\sigma_{shear} = \frac{F}{A} = \frac{F}{\pi dh} = 303 \text{ kPa (44 psi)} \tag{2}$$

The aforementioned testing indicated that both the epoxy and the tolerance ring were well-suited to handle the torques exerted by the scanner assembly. Due to schedule constraints, it was not possible to conduct additional tests in order to fully characterize both the epoxy and the tolerance ring. Despite the disadvantages mentioned in Table 4, epoxy was selected as the mating mechanism because of institutional knowledge of working with epoxies and its known flight heritage.

For future applications, we would like to reopen the trade and continue characterization of the two methods, particularly the behavior of a tolerance ring assembly subjected to random vibration. The benefits that the tolerance ring provides over epoxy, such as a simplified installation process and ease of disassembly, make the tolerance ring a desirable option. During assembly, the process had to be halted for 24 hours in order to let the epoxy cure. Had a tolerance ring been used to mate the rotor and the shaft, this portion of the assembly process would have only taken minutes. However, installation of the tolerance ring requires the use of an arbor press, which is typically not found in a clean assembly room. Another possible issue is the interaction between a steel arbor press and the high-strength permanent magnets in the rotor; a special assembly jig would likely be needed to protect the rotor from damage during installation.

Bearing Lifetime Analysis
The critical component inside the scanner assembly is the bearing, which mechanically supports the motor shaft and facilitates rotation with a low-friction lubricant. Failure of the bearing would cause the motor to seize, and lead to a science mission failure. Design requirements state that the scanner assembly motor must survive for a minimum of 6 months of continuous operation, with 12 months being the objective. Assuming continuous rotation at 60 rpm, the bearing must survive for 15.8 million revolutions to meet the 6-month nominal mission lifetime, and 31.5 million revolutions to meet the 12-months objective mission lifetime. A lifetime analysis of the bearing was performed, using equations provided by the vendor.[13] The equation used to estimate bearing lifetime is presented in Equation 3.

$$L = a_1 a_2 \left(\frac{C}{P_r}\right)^3 \tag{3}$$

L is the number of revolutions (in millions), C is the dynamic load rating of the bearing, P_r is the equivalent radial load acting on the bearing, a_1 is an adjustment factor for reliability percentage, and a_2 is an adjustment factor for ball material. The equivalent radial load is defined as the purely radial load that, if applied to the bearing, would result in the same lifetime as a bearing under radial and/or axial loading. Mathematically, it is defined by Equation 4.

$$P_r = XVF_r + YF_a \tag{4}$$

V is a rotation adjustment factor, X is a radial load factor, Y is an axial load factor, F_r is the applied radial load, and F_a is the applied axial load. The factors V, X and Y are tabulated for different values of the quantity presented in Equation 5.

$$\frac{F_a}{ZD^2}$$

(5)

F_a is again the axial load, Z is the number of balls in the bearing, and D is the ball diameter. For the bearing used in the scanner assembly, $Z = 42$, $D = 1.59$ mm (0.0626 in), and the dynamic load rating, C is 961 N (216 lbf).

The axial and radial loads were determined by assuming payload rotation in a 1-G environment, as the force of gravity acting on the payload mass is higher than any loads that will be experienced on orbit. Assuming a payload mass of 1 kg (2.2 lbm), the axial load on the bearing is 10 N (2.2 lbf). After performing the calculation for F_a/ZD^2, it was found that $V = 1.2$, $X = 0.0056$, and $Y = 2.3$. The equivalent radial load was then calculated to be 23 N (5.17 lbf):

The default lifetime equation gives the expected lifetime that 90% of the bearings in a given application will meet. To determine the expected lifetime that 99% of the bearings in a given application will meet, the a_1 factor must be changed to $a_1 = 0.21$. This provides a conservative estimate of the expected bearing lifetime. Finally, a factor of $a_2 = 0.8$ is used to account for the softer 440C stainless steel material that the balls are made of.

With all of the constants determined, the expected lifetime of the bearing could then be calculated, as presented in Equation 6.

$$L = a_1 a_2 \left(\frac{C}{P_r}\right)^3 = 13068 \text{ [x 1 million]}$$

(6)

The expected lifetime of the bearing under operation in a 1-G environment is 13 billion revolutions, which is three orders of magnitude larger than the 12-month operational objective of 31.5 million revolutions.

Thermal Validation

Thermal-vacuum testing was also used to validate the hardware. A two-day test was conducted on the flight-like Engineering Test Unit in order to characterize the performance of the full scanner assembly over predicted operating temperature ranges, and also verify the workmanship of the individual parts used in the assembly.

Thermal modeling analyses, performed in Thermal Desktop, showed a predicted operating temperature range of -5 to +25 °C for a circular 450-km orbit at 52° inclination. This conflicted with the 0 to +70 °C operational temperature range of the MicroE 1500V encoder sensor as specified by the manufacturer. Therefore, a major goal of this thermal-vacuum test was to qualify the encoder for colder temperatures in order to gain margin from the manufacturer's specifications. A procedure for the cold operating temperature qualification is shown in Figure 10.

Scenario	Chamber State		Test Procedure
TS Test Setup	Room Pressure & Temperature		• Prep chamber, test rigs, articles, + sensors • Check function + calibrate test articles + sensors • Collect benchmark data
T-0 Functional Checks	Ambient Vacuum (25 °C)		• Pump-down chamber to ~1e-05 torr • Functional checks on test articles + sensors • Command motor to 60 rpm • Collect data until thermally stable
T-1 Cold Test	Cold Vacuum (< 0 °C)		• Continue running motor at 60 rpm • Continue collecting data • Supply LN2 to bring encoder temperature to 0°C • Monitor encoder, slowly lower T to -10 °C
T-2 Thermal Cycling	Cold Vacuum (0 °C)	Hot Vacuum (70 °C)	• Command motor to 60 rpm, collect data • Complete 1+ full thermal cycles by switching between LN2 cooling and resistor heating

Figure 10. Thermal-vacuum testing procedure

The encoder performance was evaluated as a function of temperature by routing the encoder sensor's analog output to an oscilloscope outside of the thermal-vacuum chamber, and monitoring changes in signal strength (measured as voltage amplitude). As specified by the manufacturer, the signal strength is deemed nominal around 800 mV, and considered acceptable above 400 mV.

During the test, the encoder was operational through a temperature range of -8.5 to +61.5 °C, adding margin beyond the predicted operating temperature range. Though the encoder was subjected to temperatures colder than its specified operating range, the signal strength stayed within the acceptable range (shown in Figure 11). This provided the team with confidence in the encoder's performance at colder-than-specified temperatures for short periods of time (< 3 hours, or 2 orbits).
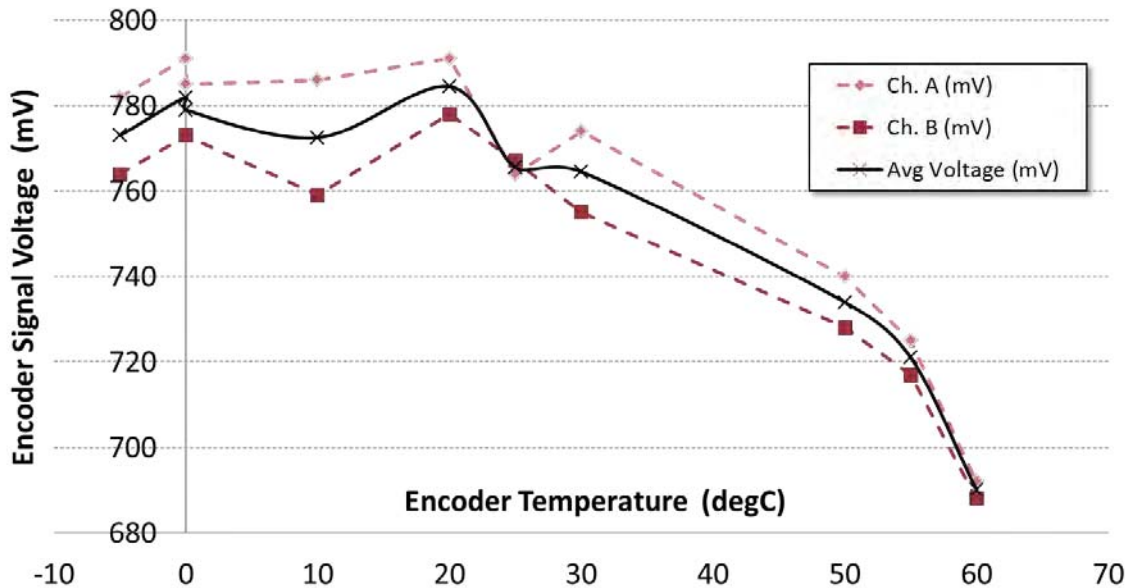

Figure 11. Encoder signal strength over expected operating temperature range

The overall scanner assembly performance was evaluated as a function of temperature by monitoring the frequency of the encoder sensor's analog output. The scanner assembly was set to spin at 60 rpm, or 7200 counts/sec (based on the 7200 gratings on the encoder disk). As set in our design requirements, this frequency should be maintained within 5% of nominal, or 360 counts/sec at 60 rpm. If one of the parts were to fail, expand, contract, or degrade as a function of temperature, this could be seen in the frequency of the encoder signal.

Over the tested temperature range of -8.5 to +61.5 °C, the encoder frequency stayed well within the 5% requirement even when tested beyond the predicted operating temperature range (shown in Figure 12), and did not show any trend as a function of temperature. This provided the team with confidence in the scanner assembly's design and performance for operation in the predicted space environment.
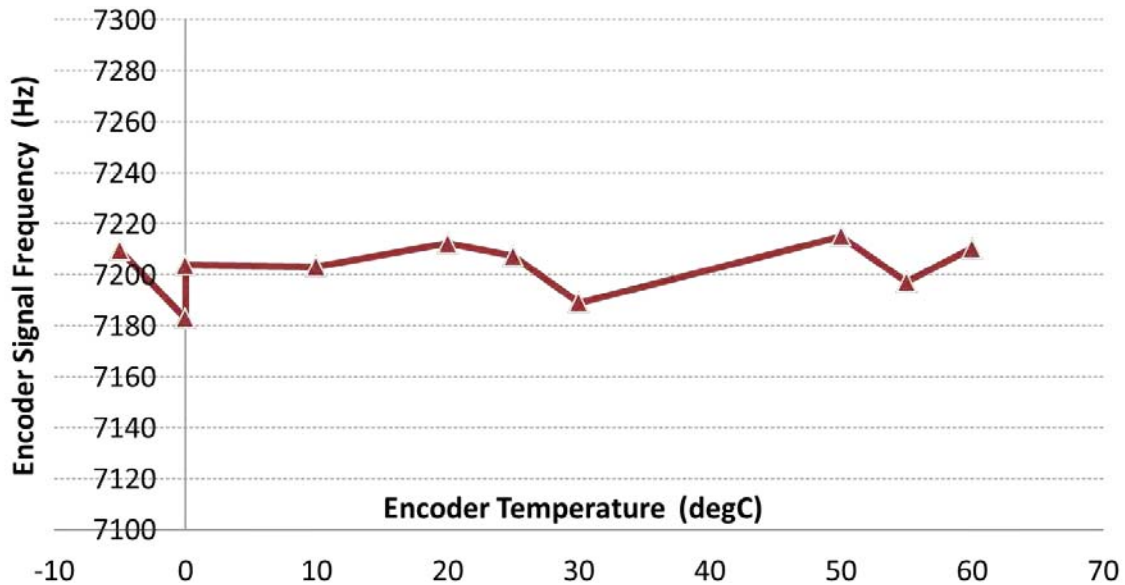

Figure 12. Scanner assembly performance over expected operating temperature range

Workmanship, however, was deemed to be an issue after the epoxy bond between the glass encoder disk and titanium mounting hub failed during bench testing several weeks after the thermal-vacuum test. Post-failure inspection determined that the epoxy did not successfully bond to the smooth glass surface of the encoder disk. As a result, greater care was taken in the surface preparation and epoxy application processes of mounting the encoder disk to the titanium hub, with the help of product engineers at MicroE Systems. The new unit was thermal-cycled and successfully tested for bond strength up to 111 N (25 lbf) prior to re-integration into the flight-model scanner assembly.

Conclusions

The MicroMAS scanner assembly is a novel new mechanism designed to provide satellites utilizing the CubeSat form factor with dual-spin functionality. The utilization of multiple COTS components allowed for successful development of a flight assembly that satisfies all of its subsystem requirements under a condensed timeline. The scanner assembly is capable of producing a continuous torque of 250 mN-m while providing sub-arcminute angular position knowledge, and allows for the transmission of 12 electrical signals between the stationary and rotating hardware. Testing has shown that the scanner assembly can functionally operate in a vacuum environment and withstand temperatures in the range of -10 to +70 °C.

The scanner assembly mechanism expands the possible science missions that can be accomplished with the low-cost CubeSat platform. After successfully passing verification of the design and performance requirements and undergoing final integration and testing within the full space vehicle, the scanner

assembly has reached TRL 8. As of this writing, MicroMAS awaits launch, scheduled for May 2014. The MicroMAS team looks forward to a successful launch, deployment, and on-orbit operation.

Acknowledgments

References

1. Wise, Evan D. "Design, Analysis, and Testing of a Precision Guidance, Navigation, and Control System for a Dual-Spinning CubeSat." Thesis, Massachusetts Institute of Technology, 2013. Found online at <http://dspace.mit.edu/handle/1721.1/82509>.
2. Wise, Evan D., et al. "A Dual-Spinning, Three-Axis-Stabilized CubeSat for Earth Observations." AIAA GNC Conference. American Institute of Aeronautics and Astronautics, 2013.
3. "The 1/2U MAI-400: A La Carte." Maryland Aerospace Inc. April 2012. Found online at <http://www.miniadacs.com/miniadacs_012.htm>.
4. "Zero Cogging Motors." *Aeroflex Motion Control Products: DC Motors*. Aeroflex Incorporated. Found online at <http://www.aeroflex.com/ams/motion/motion-motors.cfm>.
5. "Mercury 1500V Vacuum Rated Digital Output Encoders." MicroE Systems. Found online at <http://www.microesys.com/specifications/vacuum-encoders/mercury-1500V>.
6. "Airflyte: CAY-1398, CAY-1544." *Slip Ring Assemblies*. Aeroflex Incorporated. Found online at <http://www.aeroflex.com/ams/motion/motion-sliprings.cfm>.
7. "Thin Section - Radial and Gothic Arch." *Ball Bearings.* New Hampshire Ball Bearings, Inc. Found online at <http://nhbb.com/files/catalog_pages/HiTech-29-30.pdf>.
8. "Tolerances." *Reference Center.* New Hampshire Ball Bearings, Inc. Web. Accessed 12 Dec. 2012. <http://nhbb.com/reference/ball-roller-bearings/tolerances.aspx>
9. "General Environmental Verification Standard (GEVS) For GSFC Flight Programs and Projects." NASA. GSFC-STD-7000. April 2005.
10. Budynas, R. G., Nisbett, J. K., & Shigley, J. E. "Shigley's mechanical engineering design." 2011. New York: McGraw-Hill.
11. Bralower, Harrison. "Mechanical Design, Calibration, and Environmental Protection of the REXIS DAM." Thesis, Massachusetts Institute of Technology, 2013.
12. "How Tolerance Rings Work." USA Tolerance Rings, Inc. Web. Accessed 12 Dec. 2012. <http://www.usatolerancerings.com/index.php?page=how-tolerance-rings-work>.
13. "Load Ratings and Bearing Life." *Reference Center.* New Hampshire Ball Bearings, Inc. Web. Accessed 12 Dec. 2012. <http://www.nhbb.com/reference/ball-roller-bearings/load-ratings-bearing-life.aspx>.